JOURNAL OF MATERIALS SCIENCE 25 (1990) 2507–2512

Anomalous X-ray scattering study of amorphous and icosahedral $Al_{75}Cu_{15}V_{10}$ alloys

E. MATSUBARA, Y. WASEDA
Research Institute of Mineral Dressing and Metallurgy (SENKEN), Tohoku University, Sendai 980, Japan

A. P. TSAI, A. INOUE, T. MASUMOTO
Institute of Materials Research, Tohoku University, Sendai 980, Japan

Atomic structures of amorphous and icosahedral $Al_{75}Cu_{15}V_{10}$ alloys were precisely examined by the ordinary and anomalous X-ray diffraction techniques. Some distinct features of intensity profiles, and coordination numbers and interatomic distances determined from the RDF analysis, indicate the presence of the icosahedral short-range ordering clusters in the as-quenched amorphous sample and other annealed amorphous samples, which are similar to the basic atomic structure constructing the icosahedral phase. The intensity differences of the amorphous and icosahedral phases obtained in the anomalous X-ray scattering (AXS) at the Cu*K*-absorption edge suggest that copper atoms are homogeneously dispersed in the icosahedral short-range ordering clusters.

1. Introduction

The discovery by Shechtman *et al.* [1] of aluminium-based Al–Mn alloy with icosahedral point-group symmetry and long-range orientational order has stimulated many theoretical and experimental studies. Formation of an icosahedral crystal was predicted from the structure of an equilibrium phase which contains icosahedral clusters in the unit cell. In other words, formation of the icosahedral crystal formed by rapid quenching may be related with structural similarity to an equilibrium phase. Koskenmaki *et al.* [2] revealed a definite coherent orientational relationship between the α-($Al_{72.5}Si_{10.1}Mn_{17.4}$) phase and the icosahedral phase in a rapidly quenched Al–Si–Mn alloy. Audier *et al.* [3] established a close structural relationship between the Im3 Al_5CuLi_3 [4] and the Al_6CuLi_3 icosahedral phase. On the other hand, Steinhart *et al.* [5] found in molecular-dynamic simulations that icosahedral correlations increase in under-cooled liquid metals. Thus this short-range icosahedral order is preserved by sufficiently rapid quenching, which determines the structure of an amorphous state [6]. Furthermore, it was inferred that an icosahedral crystal could condense out of an undercooled liquid with structural correlations similar to those in an amorphous alloy under certain conditions [7], although the precise relationship, if any, between the icosahedral crystal and the icosahedral order in the amorphous state is not yet understood.

In a $Pd_{58.8}U_{20.6}Si_{20.6}$ alloy, an icosahedral phase is formed by annealing an amorphous phase produced by liquid quenching [8]. Similarities of the atomic structures of both the phases in a near-neighbour region were pointed out by Kofalt *et al.* [9] using the anomalous X-ray scattering (AXS) at the uranium absorption edge. Fuchs *et al.* [10] confirmed their result by X-ray and neutron scattering and H. Bretscher *et al.* [11] indicated similarities of their physical properties. Using an amorphous $Al_{86}Mn_{16}$ alloy produced by ion-beam irradiation, Lilienfield *et al.* [12] observed a transformation of the amorphous phase into an icosahedral phase with ion-beam irradiation at room temperature or with *in situ* annealing in a transmission electron microscope. A similar experiment [13] was carried out in an icosahedral Al–16 at % V alloy which is transformed into an amorphous phase by low-temperature electron irradiation in a high-voltage electron microscope. Chen *et al.* [14] attributed a pronounced prepeak, and a marked shoulder at the low Q-side of the main peak of an X-ray diffraction profile of amorphous $Al_{66}Si_{20}Mn_{14}$, to icosahedral short-range ordering clusters in the amorphous phase similar to those in α-($Al_{72.5}Si_{10.1}Mn_{17.4}$). Extended X-ray absorption fine structure (EXAFS) measurements showed a similarity to the local atomic structure around a manganese atom in icosahedral and amorphous Al–Mn alloys [15]. Also, quantitative analyses of X-ray diffraction profiles of amorphous sputtered $Al_{77.5}Mn_{22.5}$ and as-spun $Al_{56}Si_{30}Mn_{14}$ alloys confirmed the presence of icosahedral clusters, resembling those in the α-phase [16]. These experimental results imply the presence of a particular structural relationship between icosahedral crystals and amorphous alloys.

Recently, Tsai *et al.* [17] found a new and stable single icosahedral phase which is formed by crystallization of an amorphous $Al_{75}Cu_{15}V_{10}$ alloy prepared by liquid quenching. Its grain size is much larger than those of icosahedral $Pd_{58.8}U_{20.6}Si_{20.6}$ [8] or $Al_{55}Mn_{20}Si_{25}$ [18] prepared by the same method. The present authors

0022–2461/90 $03.00 + .12

systematically studied the transformation of an as-quenched amorphous $Al_{75}Cu_{15}V_{10}$ alloy into an icosahedral phase by X-ray diffraction and electron microscopy [19]. The continuous evolution of the amorphous phase into the icosahedral phase was well confirmed by comparing the intensity profiles of samples annealed below crystallization temperature. The main purpose of the present study is to report a further quantitative analysis of intensity profiles of the $Al_{75}Cu_{15}V_{10}$ alloy, including local atomic structures around copper determined in the amorphous and icosahedral samples, using the anomalous X-ray scattering (AXS) measurement at the Cu*K*-absorption edge.

2. Experimental procedures

A mixture of aluminium (99.99%), copper (99.99%) and vanadium (99.8%) was melted under argon in an arc furnace, and amorphous ribbons of about 0.02 mm thickness and 1 mm width were prepared from the alloy by a single roller melt spinning apparatus. Two samples were annealed under argon gas atmosphere for 40 800 sec (11 h 20 min) and 86 400 sec (24 h), respectively, at 620 K, which is about 100 K below the crystallization temperature determined in a differential scanning calorimetry curve [17]. A sample of the icosahedral phase was prepared by heating the as-quenched sample for 300 sec (5 min) at 820 K, just below the melting temperature 830 K. Four powder samples prepared by grinding the ribbons were used for the ordinary X-ray measurements. The anomalous X-ray scattering (AXS) measurements at the Cu*K*-edge were done for the as-quenched and icosahedral samples.

A molybdenum X-ray tube and a singly-bent pyrolytic graphite monochromator in a diffracted beam were used for the ordinary X-ray measurements. Intensity was detected by a scintillation counter with a pulse-height analyser to eliminate fluorescent radiations from the sample. A fixed-count mode was applied and at least 20 000 counts were collected at every point so that the statistical uncertainty was about $\pm 0.5\%$. The polarization correction for an ideally imperfect monochromator was applied, and the Compton scattering was corrected using the tabulated values [20, 21] with the so-called Breit–Dirac recoil factors. Observed intensities were converted into electron units by the generalized Krogh-Moe–Norman method [22] using the X-ray atomic scattering factors [23] including anomalous dispersion terms [24]. In this work, intensity data at Q values below $5\,nm^{-1}$ were smoothly extrapolated to $Q = 0$. The effect of the extrapolation and the truncation up to $Q = 153\,nm^{-1}$ is known to give no critical contribution to a radial distribution function (RDF) calculated by the Fourier transformation [25, 26].

The RDF is evaluated from a structural function $i(Q)$ in a multi-component system by the following equations.

$$4\pi r^2 \rho(r) = 4\pi r^2 \rho_0 + \frac{2r}{\pi} \int_0^{Q_{max}} Q i(Q) \sin(Qr)\, dQ \quad (1)$$

$$i(Q) = [I_{cu}^{coh}(Q) - \langle f^2 \rangle] \langle f \rangle^2 \quad (2)$$

$$\langle f^2 \rangle = \sum_{j=1}^{n} c_j f_j^2 \quad (3)$$

and

$$\langle f \rangle = \sum_{j=1}^{n} c_j f_j \quad (4)$$

where $I_{cu}^{coh}(Q)$ is the coherent X-ray scattering intensity in electron units per atom, which is experimentally determined. f_j and c_j are the scattering factor and the concentration, respectively, of the jth element. $\rho(r)$ is the averaged radial density function and ρ_0 is the average number density of atoms. Q_{max} is the maximum value of Q used for the measurement.

The AXS measurement was carried out with synchrotron radiation at the Photon Factory of the National Laboratory for High Energy Physics, Tsukuba, Japan. For details of the experimental setting and analysis used for the AXS measurements see [27]. Only some additional details which were necessary for the present study are given below. Because of particular near-edge phenomena such as XANES (X-ray absorption near-edge structure), EXAFS (extended X-ray absorption fine structure), and extremely intense fluorescent radiation on the higher-side of the edge, only the lower energy side was used for the present AXS measurement.

Incident beam energy below the Cu*K*-absorption edge was determined with an energy resolution of a few electron volts by a silicon 1 1 1 double-crystal monochromator. Since the samples were mounted on a vertically placed diffractometer, the polarization correction was ignored. The incident beam was monitored by a nitrogen-gas-flow type ion chamber placed in front of the sample. The intensity measured was converted to intensity in counts per photon by dividing the total number of photons incident on the sample calculated from monitor counts [28]. Diffracted intensities were measured by a portable pure germanium solid-state detector to collect separately the coherent intensity (corresponding to the structural information) and $K\alpha$ fluorescence from the sample. The $K\beta$ fluorescence overlapping with the coherent scattering near the absorption edge was estimated from the intensity of the $K\alpha$ radiation, and the ratio of $K\alpha$ to $K\beta$ [29], and subtracted from the coherent scattering [30]. The effect of higher harmonics diffracted by a silicon 3 3 3 plane was reduced to an insignificant level by intentionally detuning the second silicon crystal of the double crystal monochromator with a piezo electric device attached to it. The coherent intensity was corrected for absorption by the sample and air in the beam path. Compton scattering intensity was corrected in the same method as the ordinary analysis. Only the basic equations used are given below, as the details of the analysis have already been given [31, 32].

Since the incident beam energy is selected at the lower energy side of the Cu*K*-edge, the variation detected in intensity is attributed only to a change of the real part of the anomalous dispersion term f' of copper. Thus the difference between scattering inten-

sities measured at two energies E_1 and $E_2(E_1 < E_2)$ is given by

$$\Delta I_{Cu}(Q) = I(Q, E_1) - I(Q, E_2)$$
$$= c_{Cu}[f'_{Cu}(E_1) - f'_{Cu}(E_2)] \int_0^{Q_{max}} 4\pi r^2 \times \sum_{j=1}^{n} \mathrm{Re}[f_j(Q, E_1) + f_j(Q, E_2)] \times (\rho_{Cuj}(r) - \rho_{0j}) \frac{\sin(Qr)}{Qr} \mathrm{d}r \quad (5)$$

where

$$I(Q, E_j) = I_{cu}^{coh}(Q) - \langle f^2 \rangle \quad (6)$$

$\rho_{Cuj}(r)$ is the number density function for the jth atom around copper, and ρ_{0j} the average number density for the jth element. Re indicates the real part of the value in the parentheses.

The environmental RDF around copper which represents the radial distribution of atoms around copper was determined by the Fourier transform of the quantity $Q\Delta I_{Cu}$:

$$4\pi r^2 \rho_{Cu}(r) = 4\pi r^2 \rho_0 + \frac{2r}{c_{Cu}[f'_{Cu}(E_1) - f'_{Cu}(E_2)]} \times \int_0^{Q_{max}} \frac{Q\Delta I_{Cu}(Q) \sin(Qr)}{W(Q)} \mathrm{d}Q \quad (7)$$

$$\rho_{Cu}(r) = \sum_{j=1}^{n} \frac{\mathrm{Re}[f_j(Q, E_1) + f_j(Q, E_2)]}{W(Q)} \rho_{Cuj}(r) \quad (8)$$

and

$$W(Q) = \sum_{j=1}^{n} c_j \mathrm{Re}[f_j(Q, E_1) + f_j(Q, E_2)] \quad (9)$$

where $\rho_{Cu}(r)$ is the number density function around copper. By comparing the environmental RDF around copper in Equation 7 with the ordinary RDF in Equation 1, the advantage of the AXS method is easily recognized. Although six partial RDFs are overlapped in the ordinary RDF of the ternary alloy, the environmental RDF around copper is only a sum of the three partial RDFs of Cu–Al, Cu–Cu and Cu–V pairs. This energy-derivative method with the AXS technique based upon the idea of Hosoya [33] and Shevchik [34] was first used by Fuoss *et al.* [35] with synchrotron radiation under the name of differential anomalous scattering (DAS), although the principle of the method itself is unchanged.

3. Results and discussion

Fig. 1 shows the profiles of $Qi(Q)$ defined by Equation 2 for all of the samples. The fundamental features of the as-quenched sample correspond to a typical non-crystalline structure. Some distinct features are observed. For example, a prepeak appears at $Q = 15\,\mathrm{nm}^{-1}$. A marked shoulder at the low-Q side of the main peak and a small hump at $Q = 40\,\mathrm{nm}^{-1}$ are also visible. These similar features were frequently observed in aluminium-based amorphous alloys, such as Al–Si–Mn [16] and Al–Cu–V–Si–Mo [36]. In general, the presence of a prepeak has been qualitatively interpreted as one of the compound-forming behaviours, and the partial structure factor of unlike-

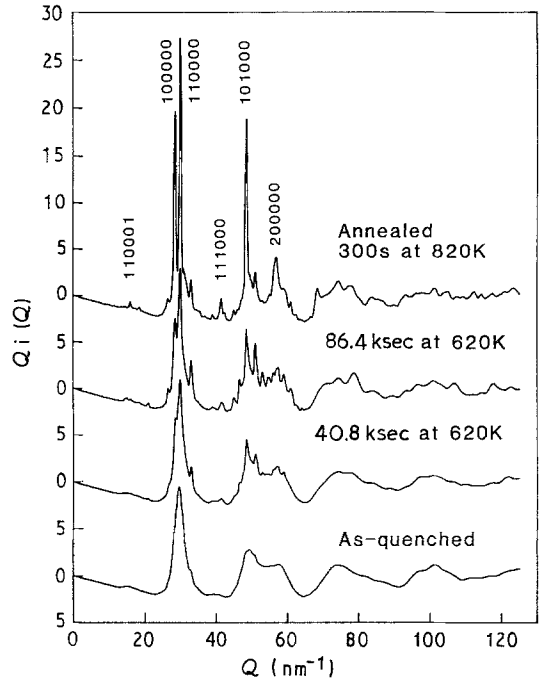

Figure 1 Function of $Qi(Q)$ of $Al_{75}Cu_{15}V_{10}$ as-quenched, and annealed for 40 800 and 86 400 sec at 620 K and 300 sec at 820 K.

atomic pairs in this type of disordered alloy is found to be a very sharp first peak with a prepeak [26, 37, 38]. In addition to the features discussed above, quite clear splitting of the second peak as well as fairly distinct oscillations at high-Q regions are rather unlike the patterns of typical amorphous alloys. These features of the patterns imply the presence of chemical short-range order in the alloys.

On annealing the as-quenched amorphous alloy, the main peak and its shoulder separate into two icosahedral peaks, which are 100000 and 110000 according to the indexing scheme of Bancel *et al.* [39]. Similarly, the small hump around $Q = 40\,\mathrm{nm}^{-1}$, the

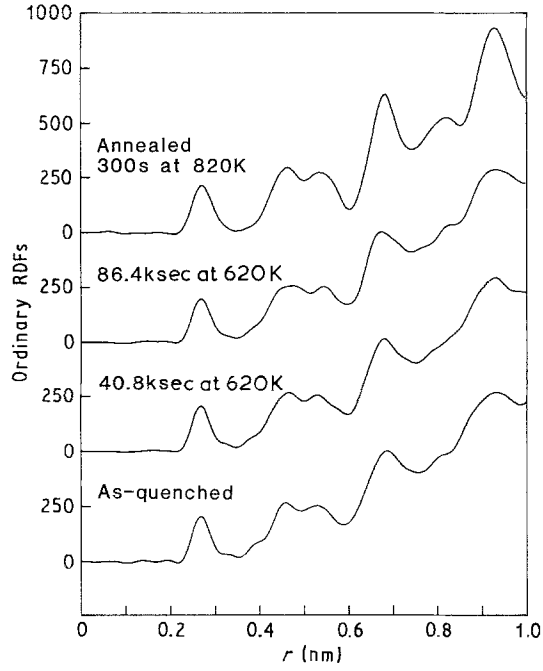

Figure 2 Ordinary radial distribution functions (RDFs) of $Al_{75}Cu_{15}V_{10}$ alloys as-quenched, and annealed for 40 800 and 86 400 sec at 620 K and 300 sec at 820 K. The density of each sample is 3.698, 3.756, 3.756 and 3.797 $\mathrm{Mg\,m^{-3}}$, respectively.

second peak and its shoulder sharpen and grow into the icosahedral peaks 110001, 111000, and 200000, respectively. This continuous growth from diffused peaks in the amorphous alloy into sharp peaks in the icosahedral phase which has already been observed in raw intensity profiles [19] gives significant evidence of the structural similarity between the icosahedral and amorphous phases.

The RDFs calculated by Equation 1 are shown in Fig. 2. The RDF of the as-quenched sample shows the first peak almost completely resolved and rather distinct oscillations over a wide range of r, compared with the RDF of a typical amorphous alloy. These oscillations are amplified in the icosahedral phase without changing their periodicity. Furthermore, it is surprising that all four RDFs up to the radial distance of 0.6 nm show an extremely similar profile. These features suggest that a local ordering structure in the as-quenched sample grows into an icosahedral structure in the sample annealed above the crystallization temperature. This is strong evidence to support the conclusion obtained from the change of intensity profiles in Fig. 1. The nearest-neighbour distance and its coordination number were estimated from the first peak of the respective RDFs. An error for the coordination number is about $\pm 8\%$ at most. These values for the four samples are summarized in Table I, with the values computed from the crystal structural data of $Al_{45}V_7$ by Brown [40].

The unit cell of $Al_{45}V_7$ consists of two kinds of icosahedra formed by aluminium atoms at vertices and vanadium atoms at their centre, and a polyhedron composed of two icosahedra sharing one of pentagonal planes with each other where aluminium atoms are located at vertices and vanadium atoms are at each centre of the two connected icosahedra. An average distance between vanadium atoms locating at the centres of these icosahedra is about 0.51 nm. The $Al_{45}V_7$ crystal data for the pairs of Al–Al, Al–V, V–Al and V–V in Table I were calculated by taking an average over all possible neighbouring pairs in the unit cell. Thus it is found that all kinds of pairs at the nearest-neighbour distance are located at about 0.27 nm. It is sometimes very difficult to determine the kind of pairs corresponding to each peak in the ordinary RDF. The sizes of constituent elements are almost equal, as in the present case. The average coordination number for all kinds of pairs corresponding to the first peak was estimated to be 11.9 from the $Al_{45}V_7$ crystal data in order to compare with those experimentally determined.

TABLE I Summary of coordination numbers, N, and interatomic distances, r.

	r(nm)	N
$Al_{75}Cu_{15}V_{10}$ alloys		
As-quenched	0.268	9.8
Annealed 40.8 k sec at 620 K	0.268	9.8
Annealed 86.4 k sec at 620 K	0.269	9.9
Annealed 300 sec at 820 K	0.272	11.4
$Al_{45}V_7$ crystal		
Al–Al	0.286	10.1
Al–V	0.270	1.8
V–Al	0.270	11.4
V–V	0.264	0.6
Average		11.9

Experimentally determined in $Al_{75}Cu_{15}V_{10}$ alloys as-quenched and annealed for 40 800 and 86 400 sec at 620 K and 300 sec at 820 K, and calculated in the $Al_{45}V_7$ crystal.

The coordination number increases with annealing time and is 11.4 in the icosahedral sample annealed for 300 sec at 820 K. On the other hand, the atomic distances only show a slight increase with annealing. The difference between the distance of the icosahedral phase and that of the as-quenched amorphous phase is only 1.5%. Since the experimental error of the atomic distance is estimated to be a few percent, the difference appears to be insignificant. Furthermore, correlation length, r, approximately estimated from an average Q-value of a prepeak in the amorphous samples is 0.524 nm by applying an empirical relation of $Qr = 2.5\pi$ [26]. This value is found to correspond to the interatomic distance between vanadium atoms located at the centre of the icosahedral clusters in the $Al_{45}V_7$ crystal. Such similarity implies that the local structures of the samples consist of icosahedral clusters which are formed by a similar atomic configuration to that in $Al_{45}V_7$, although the present samples are of a ternary alloy including copper as well as aluminium and vanadium. Accordingly, in order to obtain information about the location of copper in these icosahedral clusters, the AXS measurement at the CuK-absorption edge was carried out in the samples as-quenched and annealed for 300 sec at 820 K, that is, in the amorphous and icosahedral phases.

Anomalous X-ray scattering profiles of the amorphous and icosahedral phases are shown in Figs 3 and 4, respectively. The two profiles at the bottom of the figures are intensity profiles measured at 25 and 300 eV below the CuK absorption edge and intensity profiles of their differences are shown in the top. As shown in Fig. 3, the essential profile of the intensity difference in the amorphous phase shows a very similar

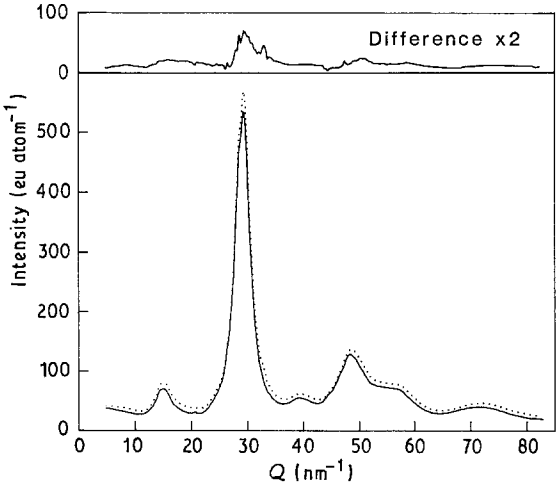

Figure 3 Differential intensity profile of as-quenched amorphous $Al_{75}Cu_{15}V_{10}$ alloy (top) determined from intensity profiles (bottom) measured at (——) 8.955 and (· · · ·) 8.680 keV, which correspond to the values of incident energy of 25 and 300 eV below the CuK-absorption edge.

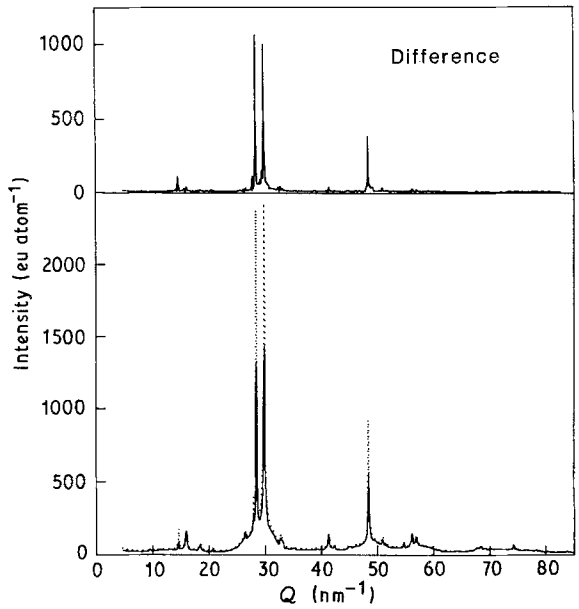

Figure 4 Differential intensity profile of icosahedral $Al_{75}Cu_{15}V_{10}$ alloy annealed 300 sec at 820 K (top) determined from intensity profiles (bottom) measured at (——) 8.955 and (····) 8.680 keV, which correspond to the values of incident energy of 25 and 300 eV below the Cu*K*-absorption edge.

feature to the original intensity pattern before taking a difference, which indicates that copper atoms are homogeneously dispersed in the icosahedral clusters. Copper atoms take both of the aluminium and vanadium sites in the icosahedral clusters. Similarly, all peaks in the intensity difference of the icosahedral phase in Fig. 4 are positive and similar to the peaks of the original icosahedral phase. It also suggests the same conclusion in the amorphous phase mentioned above. However, the following point is stressed in the intensity difference by comparing it with the original intensity for the peaks of 100000 and 110000. The peak intensities are reversed in the differential intensity profile, which indicates a possibility that copper atoms only occupy particular sites of aluminium and vanadium in the icosahedral clusters. This selective replacement of copper atoms to aluminium and vanadium sites may explain the very narrow composition range for the formation of a single icosahedral phase in the Al–Cu–V system.

Environmental RDFs around copper for both the samples computed by the Fourier transformation of the intensity difference in Equation 7, are shown in Fig. 5. For comparison, their ordinary RDFs are also shown by dotted lines in this figure. It is easily seen from Equations 1 and 7 that the absolute values of the ordinary and environmental RDFs provide the different physical meaning, and then only the peak positions give significant information in this comparison. Peak maxima of oscillations in the environmental and ordinary RDFs are surprisingly coincident with each other in both amorphous and icosahedral phases. This means that there is significant difference in the atomic configuration around copper atoms from the average atomic configuration. This result clearly leads to the same conclusion as obtained above.

In conclusion, the presence of the icosahedral short-range ordering clusters has been confirmed for the amorphous samples from the systematic X-ray scattering measurements of the $Al_{75}Cu_{15}V_{10}$ alloys. Thus it is plausible that the atomic configuration close to the icosahedral short-range ordering in the amorphous phase grows preferentially to form a quasi-crystalline structure. However, the present result is not good enough to give an understanding of the mechanism of structural evolution.

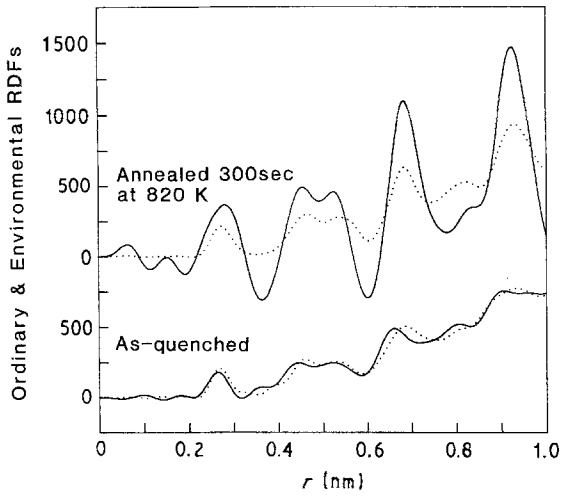

Figure 5 Comparison of environmental radial distribution functions (RDFs) around (——) copper and (····) ordinary RDFs of $Al_{75}Cu_{15}V_{10}$ alloys as-quenched, and annealed 300 sec at 820 K.

Acknowledgement

Part of this research was supported by the Mitsubishi Foundation (the research project of the anomalous X-ray scattering in 1986). We (E.M. and Y.W.) particularly wish to thank the staff of the Photon Factory, National Laboratory for High Energy Physics, Drs T. Ishikawa, M. Nomura and A. Koyama, and Professors T. Matsushita, H. Iwasaki and M. Ando.

References

1. D. SHECHTMAN *et al.*, *Phys. Rev. Lett.* **53** (1984) 1951.
2. D. C. KOSKENMAKI, H. S. CHEN and K. V. RAO, *Phys. Rev. B* **33** (1986) 5328.
3. M. AUDIER, P. SAINFORT and B. DUBOST, *Phil. Mag. B* **54** (1986) L105.
4. G. BERGMAN, J. L. T. WAUGH and L. PAULING, *Acta. Crystallogr.* **10** (1957) 254.
5. P. J. STEINHARDT, D. R. NELSON and M. RONCHETTI, *Phys. Rev. B* **28** (1983) 784.
6. S. SACHDEV and D. R. NELSON, *Phys. Rev. Lett.* **53** (1984) 1947.
7. S. SACHDEV and D. R. NELSON, *Phys. Rev.* **32** (1985) 4592.
8. S. J. POON, A. J. DREHMAN and K. R. LAWLESS, *Phys. Rev. Lett.* **55** (1985) 2324.
9. D. D. KOFALT *et al.*, *Phys. Rev. Lett.* **57** (1986) 114.
10. R. FUCHS *et al.*, *Z. Phys. B* **68** (1987) 309.
11. H. BRETSCHER *et al.*, *ibid.* **68** (1987) 313.
12. D. A. LILIENFELD *et al.*, *Phys. Rev. Lett.* **55** (1985) 1587.
13. J. MAYER *et al.*, *Z. Naturforsch.* **42a** (1987) 113.
14. H. S. CHEN, D. KOSKENMAKI and C. H. CHEN, *Phys. Rev. B* **35** (1987) 3715.
15. J. B. BOYCE, F. G. BRIDGES and J. J. HAUSER, *J. Physique* **47** (1986) C8-1029.
16. E. MATSUBARA *et al.*, *J. Mater. Sci.* **23** (1988) 753.
17. A. P. TSAI, A. INOUE and T. MASUMOTO, *Jpn J. Appl. Phys.* **26** (1987) L1994.

18. A. INOUE, Y. BIZEN and T. MASUMOTO, *Met. Trans. A* **19** (1988) 383.
19. E. MATSUBARA *et al.*, *Z. Naturforsch.* **43a** (1988) 505.
20. International Tables for X-ray Crystallography, Vol. III, edited by C. H. MacGillavry and G. D. Rieck (Kynoch, Birmingham, 1968) p. 250.
21. D. T. CROMER, *J. Chem. Phys.* **50** (1969) 4857.
22. C. N. J. WAGNER, H. OCKEN and M. L. JOSHI, *Z. Naturforsch.* **20a** (1965) 325.
23. International Tables for X-ray Crystallography, Vol. IV, edited by J. A. Ibers and W. C. Hamilton (Kynoch, Birmingham, 1974) p. 99.
24. D. T. CROMER and D. LIBERMANN, *J. Chem. Phys.* **53** (1970) 1891.
25. C. N. J. WAGNER, *J. Non-Cryst. Solids* **31** (1978) 1.
26. Y. WASEDA, "The Structure of Non-Crystalline Materials" (McGraw-Hill, New York, 1980) p. 60.
27. Y. WASEDA, E. MATSUBARA and K. SUGIYAMA, *Sci. Rep. RITU A* **34** (1988) 1.
28. E. MATSUBARA *et al.*, *Trans. Jpn Inst. Metals* **29** (1988) 697.
29. N. V. RAO *et al.*, *Physica* **138C** (1986) 215.
30. S. AUR *et al.*, *Solid State Commun.* **48** (1983) 111.
31. Y. WASEDA, "Novel Application of Anomalous X-ray Scattering for Structural Characterization of Disordered Materials" (Springer-Verlag, New York, 1984) p. 84.
32. E. MATSUBARA *et al.*, *Z. Naturforsch.* **43a** (1988) 181.
33. S. HOSOYA, *Bull. Phys. Soc. Jpn* **25** (1970) 110.
34. N. J. SHEVCHIK, *Phil. Mag.* **35** (1977) 805.
35. P. H. FUOSS *et al.*, *Phys. Rev. Lett.* **46** (1981) 1537.
36. S. GARCON *et al.*, *Scripta Metal.* **21** (1987) 1493.
37. H. F. BUHNER and S. STEEB, *Z. Naturforsch.* **24a** (1969) 428.
38. S. STEEB and R. HEZEL, *Z. Metallkde* **57** (1963) 374.
39. P. A. BANCEL *et al.*, *Phys. Rev. Lett.* **54** (1985) 2422.
40. P. J. BROWN, *Acta Cryst.* **12** (1959) 995.

Received 17 January
and accepted 16 August 1989